Eco-Friendly Organic Perovskite Photovoltaic -Based Hole Transport Layer for Tin Mono Sulfide Solar Cell: A Numerical Simulation Approach via SCAPS-1D Application

Sunil Kumar[1], Vijay Kumar Mishra[2], Divyanjalee Kumari[3], Neelabh Srivastava[3], Rajanish N. Tiwari[4], and Arvind Kumar Sharma[3*]

[1]Department of Physics, Government Post Graduate College, Bisalpur, Pilibhit 262201, U.P., India
[3]Department of Physics, Institute of Applied Sciences & Humanities, GLA University, Mathura- 281406, U. P., India.
[3]Department of Physics,School of Physical Sciences, Mahatma Gandhi Central University, Motihari-845401, Bihar

[4]Department of Chemistry, School of Physical Sciences, Mahatma Gandhi Central University, Motihari-845401, Bihar

ABSTRACT

Because solar energy is so abundant, it is gradually replacing fossil fuels as one of the main energy sources. It is measured one of the mainly capable renewable power sources due to its ample supply, adaptability, and ecological advantages. An electrical device that transforms light energy into electrical energy is called a solar cell.The photoelectric effect is the basis for its operation. A photovoltaic cell, or P.V. cell, is another term for a solar cell. A P-N junction diode is the primary component of a solar cell. This study covers perovskite solar cells based on chalcogenides.The presentation of perovskite solar cells, a relatively new photovoltaic technology, has enhanced recently. This paper uses the SCAPS-1D simulator to study an n-p-p+ perovskite solar cell. The FTO/TiO_2/SnS/$MASnI_3$/Au photovoltaic cell structure has a power transfer efficiency of > 27.95%. A number of materials were proposed as hole and electron carrying layers (HTL and ETL) to improve its performance. But this paper discusses the solar cell structure perovskite HTL(P^+-$MASnI_3$) /absorber material (chalcogenide material) p-SnS/inorganic ETL(n-TiO_2)/left contact (Au)/right contact (FTO). There are three layers in this structure, with the thicknesses of Au/p^+ $MASnI_3$/p-SnS/n-TiO_2/FTO being 0.50 µm, 0.900 µm, and 0.020 µm, respectively.

Key words: Perovskite materials; photovoltaic cell; recombination; efficiency

***Corresponding author:** arvindkumar@mgcub.ac.in;

1. Introduction

The sun provides a lot of energy and is a natural, sustainable energy source.. By converting this energy into electrical energy with solar cells, electrical devices can use it properly, without polluting the environment or harming living beings. Solar cells have three basic generations. In 1906, the San Francisco earthquake, which registered a magnitude of 7.8, discharged an rough and ready 1017 joules of energy, comparable to the energy output of the sun in one second. [1] The Earth's reserves hold 3 trillion barrels of oil, which equate to 1.7 × 10^^{22} joules energy, a quantity which the sun can supply in just 1.5 days. In contrast, the 4.6 × 10^^{20} joules consumed by humanity each year can be replenished by the sun in merely one hour. Approximately 1.2×10^{25} terawatts of energy are continually produced by the sun, which is significantly superior to any former non-renewable energy or renewable source. This energy is far further than the roughly 13 terawatts of energy needed by humans. Twenty terawatts of electricity, or almost double the world's fossil fuel usage, including multiple nuclear fission reactors, could be produced by covering 0.16% of Earth's area with 10% effective solar cells [1].Although solar energy is plentiful, very little of it is directly utilized to fuel human endeavors.Fossil fuels provide between 80% and 85% of our energy. Greenhouse gasses and other dangerous environmental pollutants are produced by these non-renewable, rapidly decreasing resources. [2] A

significant amount of greenhouse gases, such as CO_2, are released by fossil fuels. The overuse of fuels to satisfy the constantly growing demands of human civilization has directed to an enlarge in these emissions. The prioritization of renewable energy sources is admirable, and owing to its flexibility, infinite supply, and environmental sustainability, solar power is by far the most preferred energy source [1].Our adoption of renewable energy sources for the future has also been prompted by the finite nature of fossil fuels.
The plot of yearly oil output vs year, with 2% annual growth and fall rates, is displayed in Figure 1. The necessity for an alternate energy source is highlighted by the fact that these predictions indicate a very sharp reduction in this resource beyond 2016. [3] With an yearly increase level of 41% over the past five years, the rapidly expanding solar cell business is developing into a very lucrative investment for enterprises [4]. One of the biggest obstacles to solar power being a major energy source has been its high cost and low conversion efficiency. Solar power is becoming an increasing power source globally because to new techniques for utilizing the whole range of the sun's wavelengths, multijunction solar cells (heterojunctions and homojunctions), and novel resources for solar cell production.[5] Here, I'll be talking about "Optimization and Simulation study of Tin Sulfide Chalcogenide based perovskite ($MASnI_3$) heterojunction Solar Cell by means of SCAPS-1D." Chalcogenide materials are inorganic compounds that include the elements S, Se, and Te. The role of temperature in affecting the physicochemical characteristics of deposited SnS layers, which change through variations in resource and substrate temperature, has been explored experimentally [6].

A maximum efficiency of 27.95% is also revealed by numerical study of SnS material [7]. Although SnS plans include not yet exceeded 4.6% efficiency, numerical analysis indicates that SnS is a good choice for future PV technology [7]. Defects and contaminants in SnS layers resulting from the evidence process and the self-oxidation of Sn^{2+} to Sn^{4+} might be the cause of SnS's decreased efficiency.[7] Perovskite materials consist of a mixture of halide elements along with organic-inorganic molecules. The conventional formula for these materials, characterized by a three-dimensional structure, is ABX3, where A is an organic ion like formamidinium ($NH{=}CHNH^{3+}$), or methylammonium (CH_3NH^{3+}), X represents a halogen ion (I-, Br-, or Cl-) and B is an inorganic cation (Pb^{2+}, Sn^{2+}) [8]. Hima et al. recently used ATLAS software to optimize layer thickness in order to create TiO_2-based PSCs with the maximum efficiency.[8] Based on both investigational and theoretical studies, $CH_3NH_3I_3$ ($MASnI_3$) possesses an most select 1.3 eV band gap and is measured a promising alternative to LHPSC. Its narrower band gap may allow it to absorb a broader array of the visible light spectrum related to LHPSC. Consequently, a heterostructured planar structure solar cell based on tin (Sn) perovskite has been created [9–11]. The oxidation of Sn from Sn^{+2} to Sn^{+4} in the air is the main drawback of Sn-based perovskite, which restricts the device's performance. Among the highest efficiencies in Tin Sulfide chalcogenide-based perovskite solar cells documented to far are based on TiO_2 as ETL. TiO_2 is the ETL material that I have chosen as a result. The layers of a chalcogenide-based perovskite solar cell structure, n-TiO_2 ETL (another n-SnO_2, n-ZnO) /p-SnS absorber /p+-MASnI3 perovskite HTL /Au, have been improved this work by means of SCAPS-1D software as the simulation tool. In order to achieve the maximum efficiency, the article stands out as a unique approach in optimizing the width of each layer of a TiO_2-based perovskite solar cell. The characteristics for this structure (front contact FTO/n-TiO_2/p-SnS/p+-$MASnI_3$/Au (back contact)) are eta%27.95, V_{oc}(V) 0.99, J_{sc} (mA/cm^2) 33.5, and FF (%) 83.8. TiO_2 is employed as the ETL in solar cells with some of the maximum reported efficiency to date. However, in order to generate the crystalline rutile phase, TiO_2 must be annealed at a high temperature (500 degrees Celsius), which prevents solar cells from being used in flexible devices. TiO2 is also UV-unstable and has limited electron mobility. Since FTO and Au function as electrodes, I have employed them as front and back contacts in this device construction. because of the beginning of the electron flow. As a result, the circuit begins to produce current.

2. ***Variation in device structure of the modeled heterojunction solar cell and numerical simulation***

Currently, numerical simulation techniques make it simple to build a structure with regulated dimensions that best suits the intended outcomes and analyze the outcomes of the constructed structure. To get the required material or device attributes, numerical simulation techniques allow control over changing any or many of the device's dimensions and constituents. Additionally, without requiring any effort in experimental arrangements or related inputs, numerical simulation methods improve thoughtful of the impact of various parameters on designing a particular device and results. This is because experiments need a proper laboratory with a good plan, a lot of time, energy, and resources, as well as the use of chemicals, etc. Furthermore, a single experiment could not produce the expected findings, necessitating the experimental iteration approach for approximation, which clearly raises the input requirements as previously mentioned. On the other hand, these specifications and inputs for iteration and approximation do not need to be stated at the beginning of numerical simulation methods. Only the last experiment has to be conducted in the lab for additional verification and application because the numerical simulation findings are nearly identical to the experimental values. However, the final experiment and the surrounding factors need to be repeated in order to verify the experimental results.

This study employs the one-dimensional solar cell capacitance simulator (SCAPS-1D version 3.3.10) to design a solar cell and examine its electrical and optical characteristics, aiming to attain enhanced power conversion efficiency. Created by the "Department of Electronic and Information Systems (ELIS) at the University of Gent in Belgium", SCAPS-1D is a well-respected and identical tool for solar imitation research [12]. The SCAPS-1D software utilizes Poisson's equation, along with the charge carrier and electron and hole continuity equations. A solar cell can accommodate as many as seven different layers to provide a diverse range of options [13–14]. SCAPS simulates the processes involved in solar capture, the generation of electron-hole pairs, their transit, and extraction through fundamental equations. This versatile tool permits the incorporation of a broad spectrum of unique material parameters required for the manufacturing of a specific solar device. The outputs derived from the simulation are then used to analyze their effects on device functionality and to compile vital insights into key solar character, together with the density of material defects, their location and intensity, combine again phenomena and the arrangement of bandgaps across device layers, among other considerations. To conclude, the use of SCAPS facilitates the resolution of various critical issues pertaining to materials science and device physics.
For a semiconductor, the poison equation may be expressed as –

$$\nabla^2\phi = \frac{q}{\epsilon}(n - p + N_A + N_D) \text{ .... (1)}$$

where n and p denote the free carrier densities of electrons and holes, respectively, and ε represents the dielectric constant.
N_A denotes the acceptor concentration, N_D signifies the donor concentration, and ε refers to the electrostatic potential. The continuity equation pertinent to a semiconductor can be expressed as

$$\nabla J_n - q\frac{\partial n}{\partial t} = +qR \text{ ....(2)}$$

$$\nabla J_p + q\frac{\partial p}{\partial t} = -qR \text{ .... (3)}$$

Here rate of carrier recombination is R, the current density for electrons,($J_{n)}$ and J_p is the current density for holes. The displacement of minority charge carriers instigated by the electric field, together with the distribution current resulting from the attention gradient, are the two principal determinants of current flow within semiconductors.

The continuity equation provides the drift diffusion recent relative as

$$J_n = qn\mu_n\epsilon + qD_n\frac{dn}{dx} = q\mu_n\left(n\epsilon + \frac{kt}{q}\frac{dn}{dx}\right) = \mu_n n\frac{dE_{Fn}}{dx} \text{ .... (4)}$$

$$J_p = qp\mu_p\epsilon + qD_p\frac{dp}{dx} = q\mu_p\left(p\epsilon + \frac{kt}{q}\frac{dp}{dx}\right) = \mu_p p\frac{dE_{Fp}}{dx} \text{ .... (5)}$$

mobilities of electrons (μ_n) and holes (μ_p) are denote μ_n and the correspondingly, while current densities for holes and electrons represent by J_p and J_n. Diffusion coefficients for holes and electrons are D_p and D_n, respectively, and quasi-Fermi levels for electrons and holes are specified by E_{Fn} and E_{Fp}.[15–18]. The SCAPS-1D program utilizes the Pauwells-Vanhoutte model [19], that considers the valence bands and conduction of together semiconductors in the interference, for analyzing recombination. In this study, the A.M.1.5_1_sun.spe solar light spectrum, characterized by an occurrence power density of 1000 W/m2, was employed for all simulations [20–21]. The SCAPS-1D application permits the incorporation of seven semiconductor layers, without the face and back connections; however, in this investigation, we decided to utilize four layers. The key material parameters necessary for simulation for each layer, along with the metal work functions for the face and back interactions, were provided via the SCAPS-1D (v3.3.10) description plate. The device's design is deliberate as Au/p+ $MASnI_3$/p-SnS/n-TiO_2/FTO. The foremost layer of the device is MASnI3, which serves as the hole transfer layer (HTL), followed by SnS, that doings as the absorber layer, n-TiO_2 as the electron transport layer (ETL), FTO as the transparent conducting oxide (TCO) as the fourth layer, and Au (gold) as the reverse contact, which has a metal work function of 5.2 eV [23–24]. Additionally, with a metal work function of 4.4 eV, FTO serves as the front contact.

[22]. The input parameters for the suggested solar cell design are outlined in Table 1 [25–29]. The area illuminated from the front contact was subjected to the A.M.1.5_1_sun.spe (Air Mass 1.5 Global Spectrum) by an incidence power of 1000 W/m^2. Figure 1 presents the schematic design, energy band alignment figure, and energy band diagram of the modeled heterojunction photovoltaic cell (HPVC) based on tin sulfide chalcogenide using the $MASnI_3$ HTL.

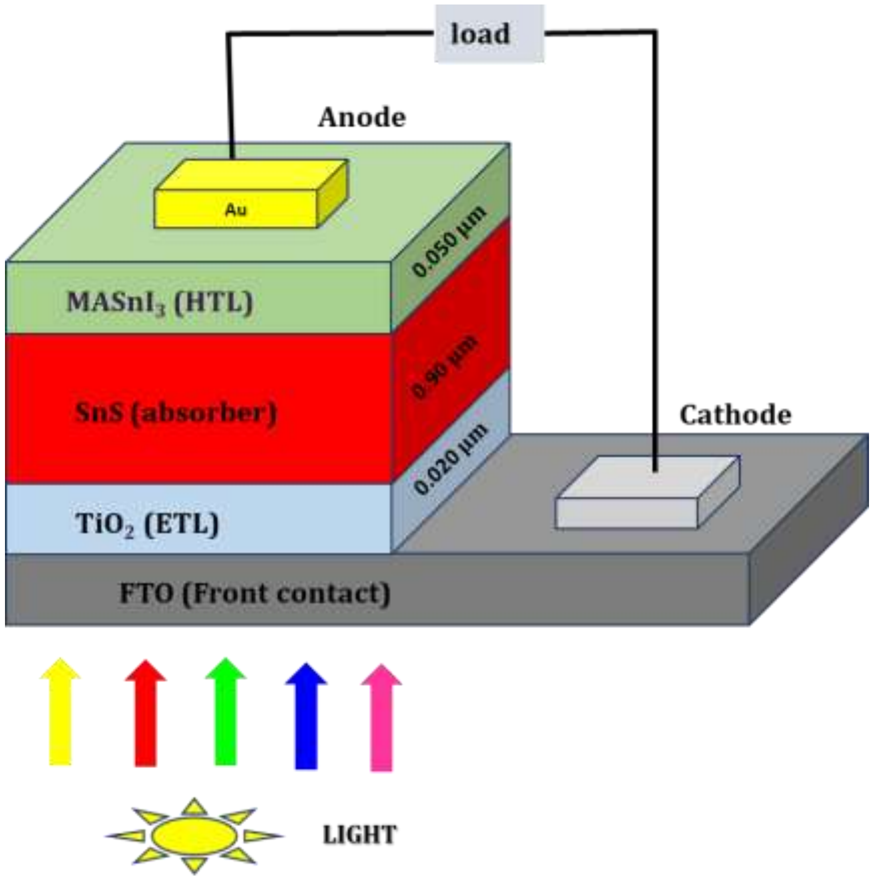

Figure 1:*Representation of the designed chalcogenide-based solar cell structure*.

3.Results and discussion

3.1 Device Simulation Technique

The material characteristics for each layer of the chalcogenide-based perovskite solar cell are used to simulate the device construction. Figures 2 and 3 depict the primary screen that appears once SCAPS is run.

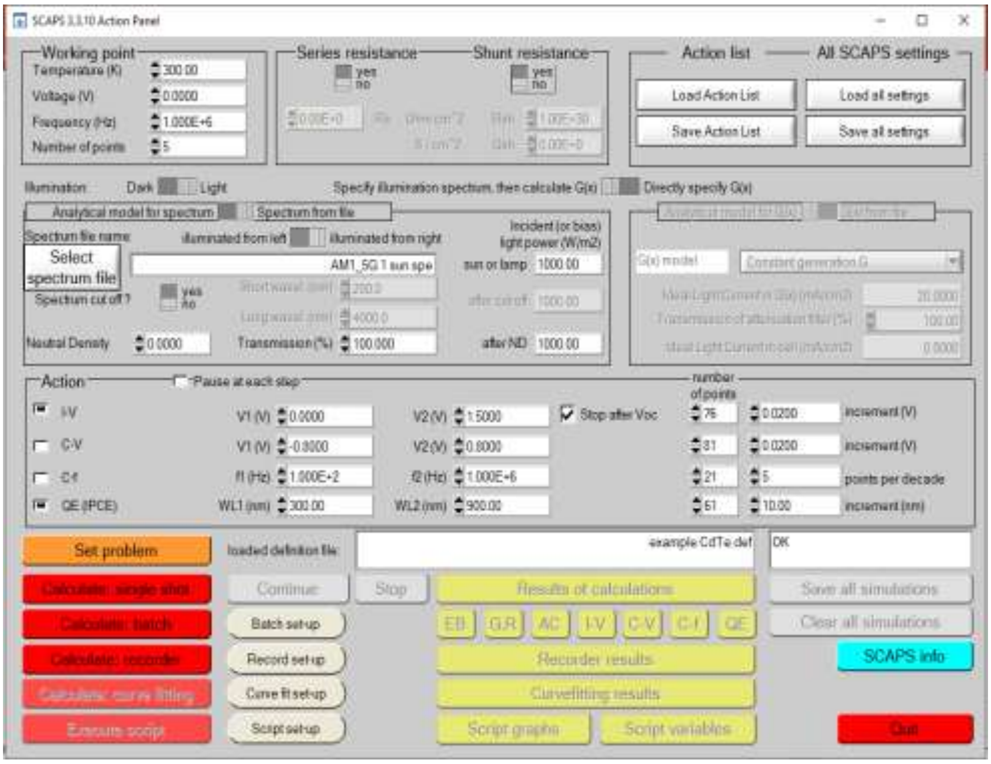

Figure 2: *Action Panel of SCAPS-1D Application*

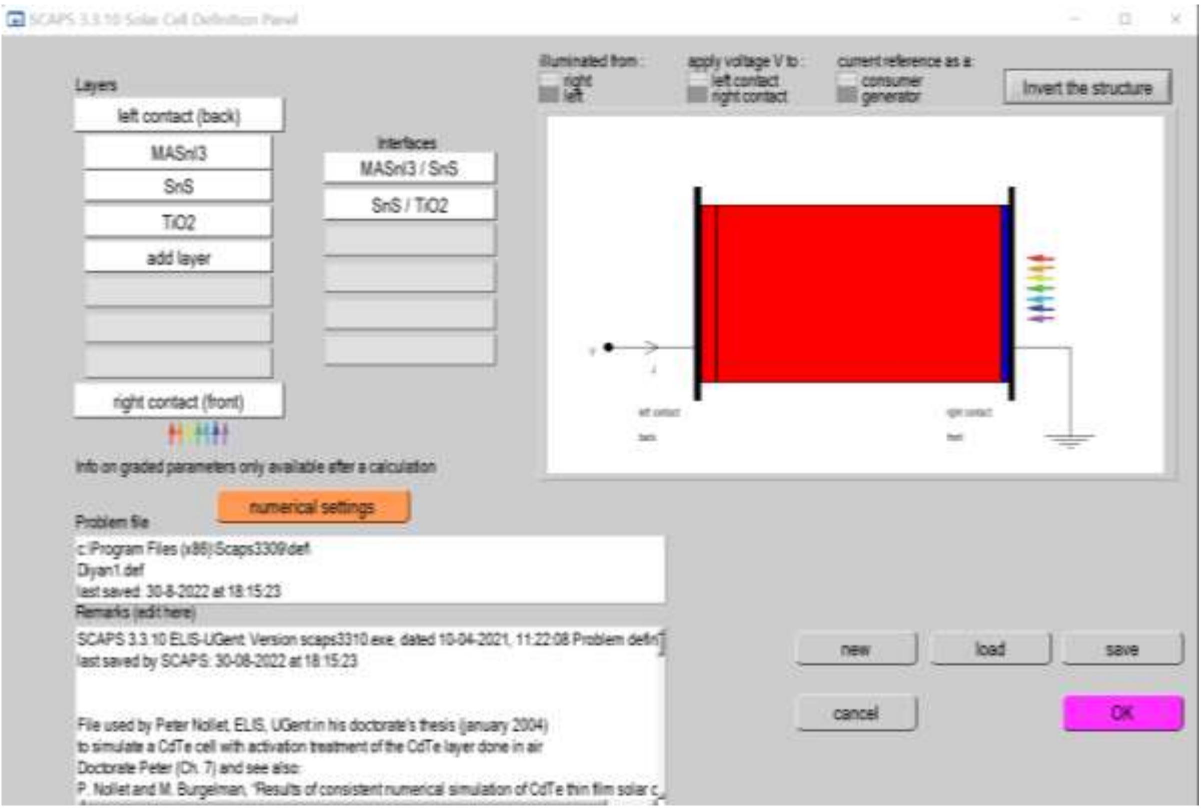

Figure3: *An illustration of a modelled solar cell device structure*

3.2 Device Simulation Parameters

Table 1: *Materials Parameters used in the imitation of a Solar Cell. [25-29]*

Material Parameter	MASnI3 (HTL)-layer1	SnS(absorber)-layer2	TiO2 (ETL)-layer3
Thickness (nm)	0.05	0.9	0.02
Band gap (eV)	1.3	1.34	3.2
Electron Affinity (eV)	4.170	4.2	4.0
Dielectric permittivity	6.5	13.0	9.0
CB effective density of states (cm^{-3})	1×10^{18}	1.8×10^{18}	2.0×10^{18}
VB effective density of states (cm^{-3})	1×10^{19}	4.76×10^{18}	1.1×10^{19}
Electron thermal velocity (cm/s)	1×10^{7}	1×10^{7}	1×10^{7}
Hole thermal velocity (cm/s)	1×10^{7}	1×10^{7}	1×10^{7}
Electron mobility (cm^2/Vs)	1.6	15	20
Hole mobility (cm^2/Vs)	1.6	100	200
Shallow donor density N_D (cm^{-3})	0	0	1×10^{18}
Shallow acceptor density N_A (cm^{-3})	1×10^{19}	1×10^{17}	0
Defect density N_t (cm^{-3})	2×10^{17}	1×10^{14}	1×10^{15}

Table 2: ***Material parameters for interface defect layers.***

Parameters	ETL (TiO_2)/SnS (chalcogenide) interface	SnS/ HTL $MASnI_3$(Perovskite) interface
Defect type	Neutral	Neutral
Capture cross section electrons (cm^2)	1×10^{-19}	1×10^{-19}
Capture cross-section holes (cm^2)	1×10^{-19}	1×10^{-19}
Total density	1×10^{10}	1×10^{10}

3.3 Variation of I-V features of chalcogenide-based solar cell

The final enhanced results of Fill factor, Jsc (mA/cm^2), Voc (V), and (%) without HTL ($MASnI^3$) are shown in Figure 4(a-b). The final optimized results of Fill factor, Jsc (mA/cm^2), Voc (V), and η with HTL ($MASnI_3$) and (b) quantum effectiveness of the chalcogenide SnS-based perovskite solar cell are shown in Figure 5(a).

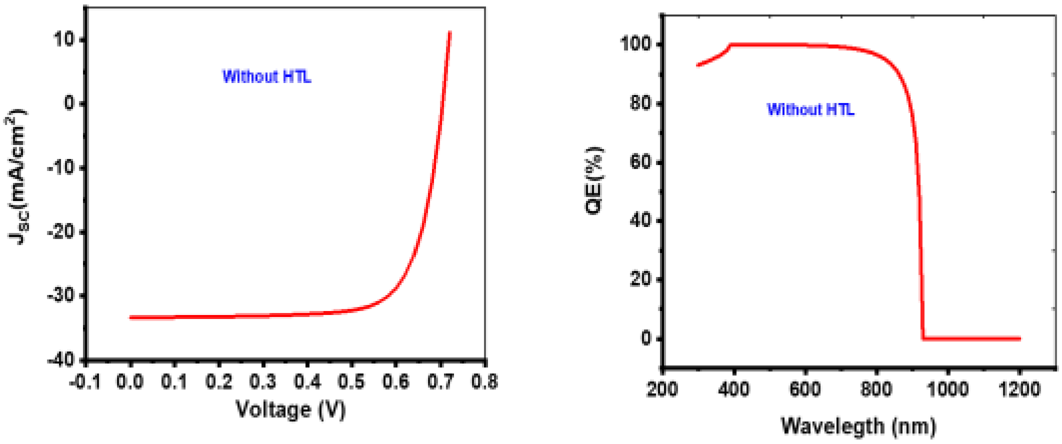

Fig. 4: (a) *J-V characteristics of the SnS-based SC, (b)QE graph Quantum efficiency*

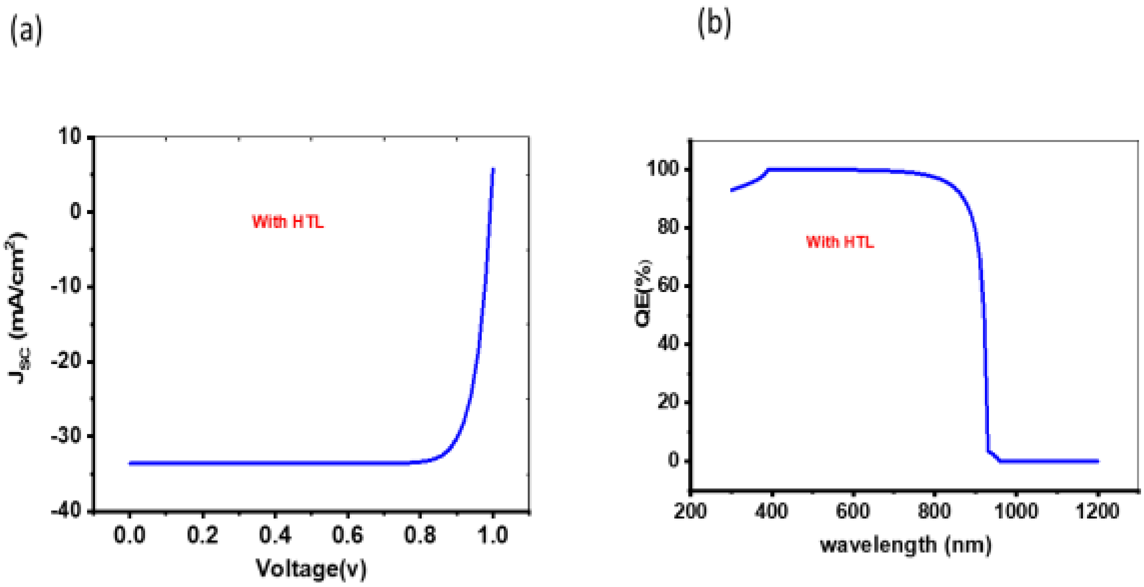

Fig. 5 (a): *J-V characteristics of the SnS-based SC. with HTL and (b) Quantum efficiency (300-1200nm)*

Table 3: Optimized Value of V_{oc}, J_{sc} (mA/cm^2), FF (%), eta (%)

V_{oc} (V)	**0.704**
J_{sc} (mA/cm^2)	**33.37**
FF (%)	**74.38**
η (%)	**17.38**

3.4 Effect of thickness of SnS (Absorber Layer) on Solar cell Parameters

Figure 6 illustrate the contact of the absorber layer thickness, specifically using SnS chalcogenide material, on various electrical parameters including V_{oc}, J_{sc}, fill factor, and efficiency. With the width advancing from 100 nm to 900 nm, the efficiency escalates, only to witness a small drop from 900 nm to 2 µm. This enhancement in efficiency can be attributed to the rise in current density that accompanies the increase in absorber layer thickness. A thicker absorber layer facilitates improved carrier generation due to greater exposure of the absorber material to light [22]. The peak efficiency is achieved at 900 nm.

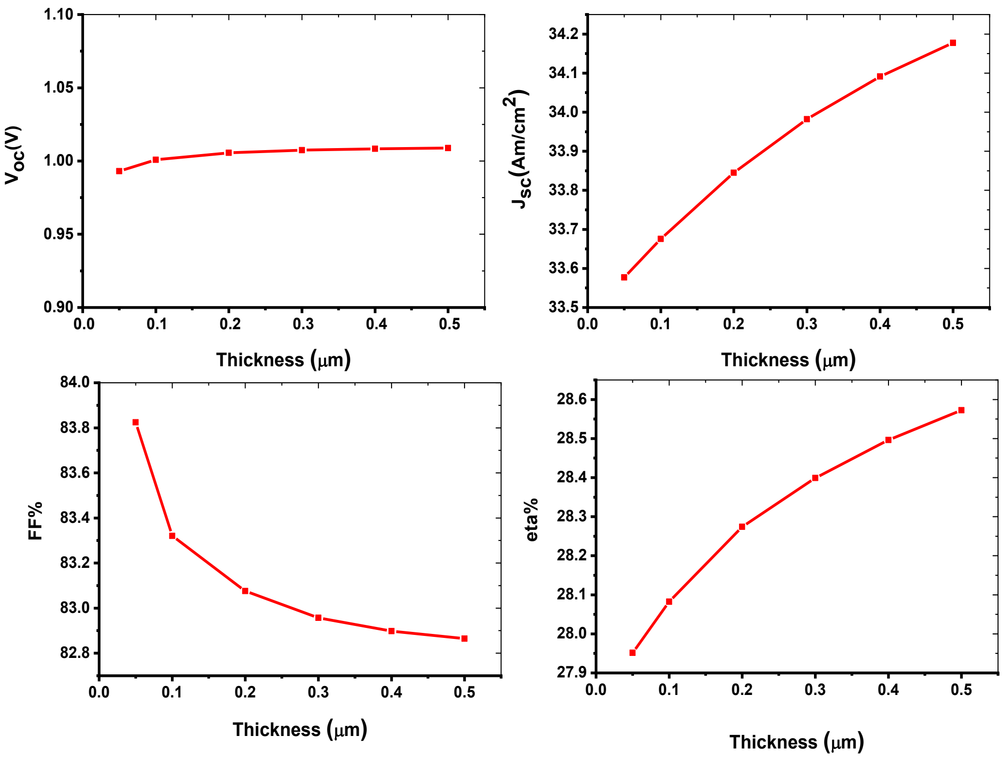

Figure 6: *Variation of efficiency, fill factor, J_{sc}, and V_{oc} with respect to the width of the absorber layer (SnS).*

3.5 Influence of thickness of $MASnI_3$ (HTL) on Solar Cell Parameters

The role of the HTL layer width in influencing the act and productivity of Chalcogenide SnS-created perovskite solar cells is illustrated in Figure 7. In this circumstance, $MASnI_3$ perovskite is employed as a conventional hole transfer material for these solar cells. The HTL thickness ($MASnI_3$) is modified from 50 nm to 500 nm, corresponding to the width of the ETL (TiO_2) inorganic material. An HTL thickness of roughly 0.50μm yields the maximum efficiency of 27.95%. As the thickness transitions from 100 nm to 500 nm, the fill factor also increases. The most effective HTL width is 500 nm, with the related solar cell performance metrics being Jsc of 33.58 mA/cm^2, V_{oc} of 0.99, a fill factor of 83.82%, and an efficiency of 27.95%.

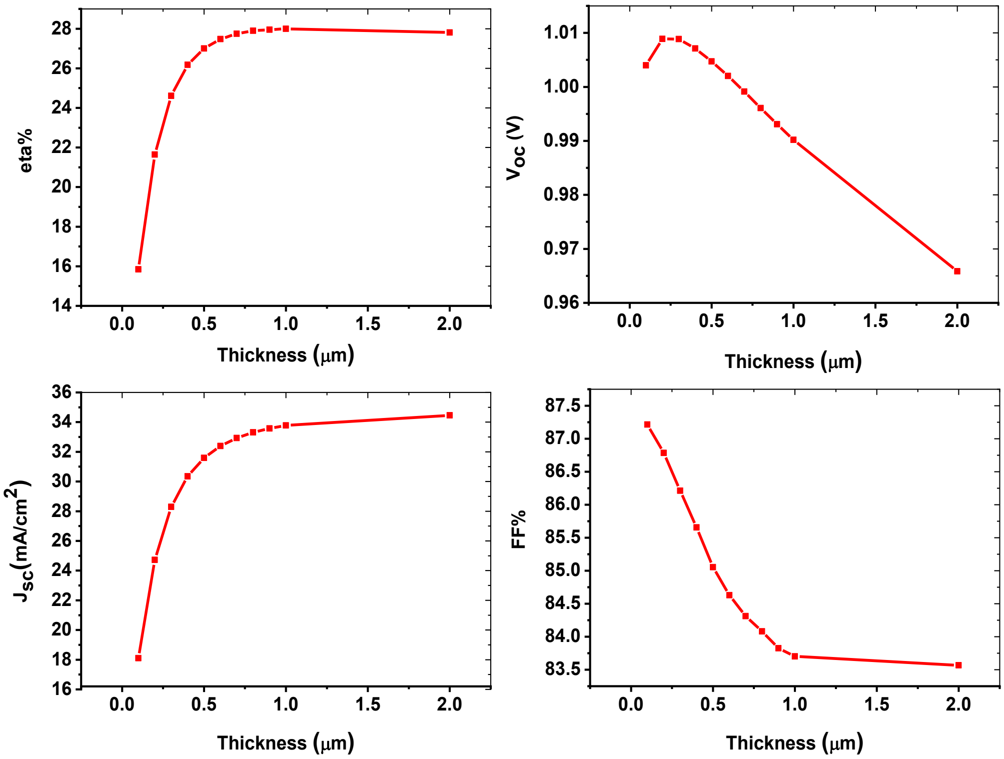

Figure 7: *Variation of efficiency, fill factor, J_{sc}, and V_{oc} with against to the thickness of HTL($MASnI_3$).*

3.6 Impact of thickness of TiO_2 (ETL) on Solar cell Parameters

The control of the thickness of the ETL (TiO_2) layer on the properties of chalcogenide SnS-based perovskite solar cells is illustrated in Figure 8. The findings indicate that although Jsc (mA/cm^2) shows minor variations as the width increases from 20 nm to 60 nm, the efficiency (%), fill factor (%), and V_{oc} (V) remain unchanged. This suggests that the electrical properties of the chalcogenide-based perovskite solar cell are not considerably affected by the electron transport layer.

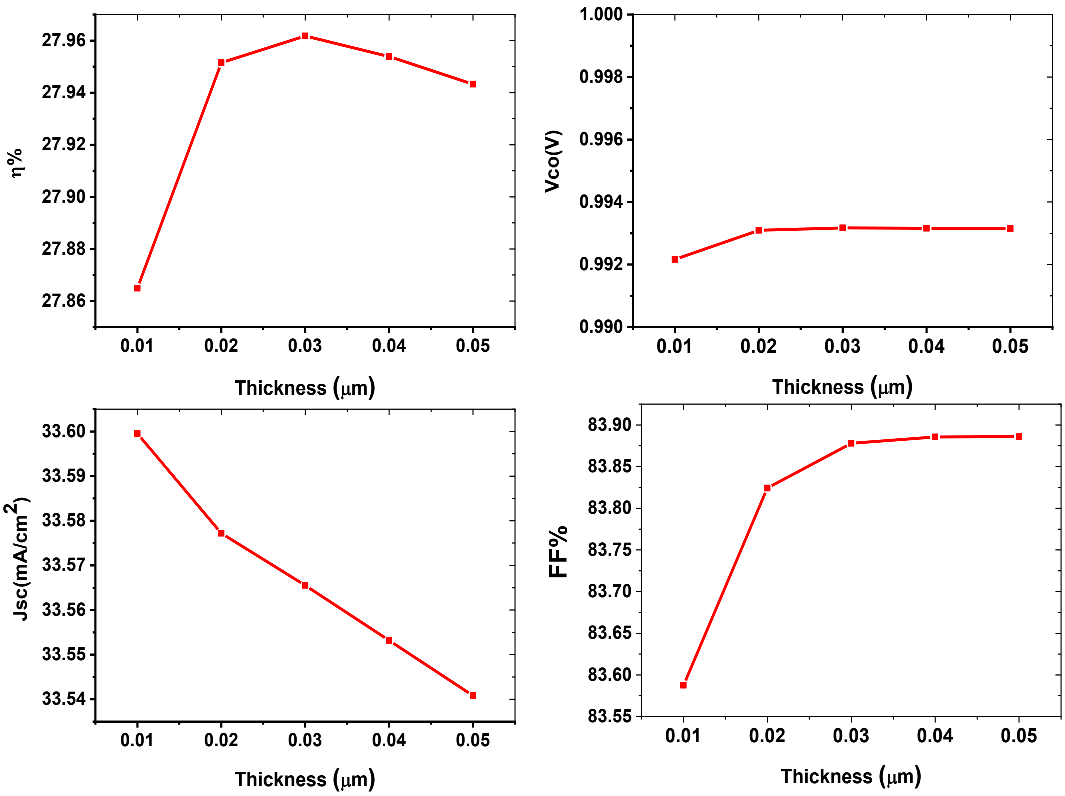

Figure 8: *Variation of efficiency, fill factor, Jsc, and Voc with respect to the thickness of ETL(TiO_2).*

3.7 Effect of Doping density N_A of HTL $MASnI_3$ on Solar cell Parameters

The HTL is essential for the effective movement and group of charge carriers, which is crucial for enhancing solar cell presentation. In adding to its part in mitigating the increase of minority charge carrier (e) that contributes to recombination within the heterojunction of the photovoltaic cell, the active HTL is responsible for the transfer of holes produced by photons starting the active absorber layer to the electrode. This function greatly boosts the overall performance of photovoltaic cells utilizing Chs tin mono sulfide. In this statement, we have observed the effects of doping density and the width of HTL $MASnI_3$ on photovoltaic cells that are based on Chs tin mono sulfide, while maintenance all other parameters unchanged. The role of doping (NA) on the output electrical characteristics is represented in Figure 9. It is apparent that the Voc slightly increases up to 1020 cm^{-3} and then relics constant, while the J_{sc} is almost unchanged. In summary, centered on the modifications, the fill factor and productivity values rise linearly up to 1018 cm^{-3}, after which they increase nonlinearly until 1021 cm^{-3}. This can be expressed by the rise in carrier attention at high doping levels, that results in a greater migration of holes towards the SnS/$MASnI_3$ interface. Minority electrons do not recombine with all of the holes in the HTL, which improves the fill factor (FF) and efficiency (η). Additionally, as the doping density increases, the fill factor enhances due to increased resistivity at the boundary, which reduces series resistance and added boosts the conductivity of the HTL. Furthermore, significant doping elevates the conductivity of the hole-transport layer, thereby refining the entire charge transfer process. Additionally, it creates an ohmic contact between the electrode and HTL, which is critical for effective charge collection, and improves boundary resistance by lowering absorber layer traps, which is necessary for effective hole extraction. The energy levels between the absorber and the hole-transport layer may be adjusted with the help of the hole-transport layer's ideal doping.

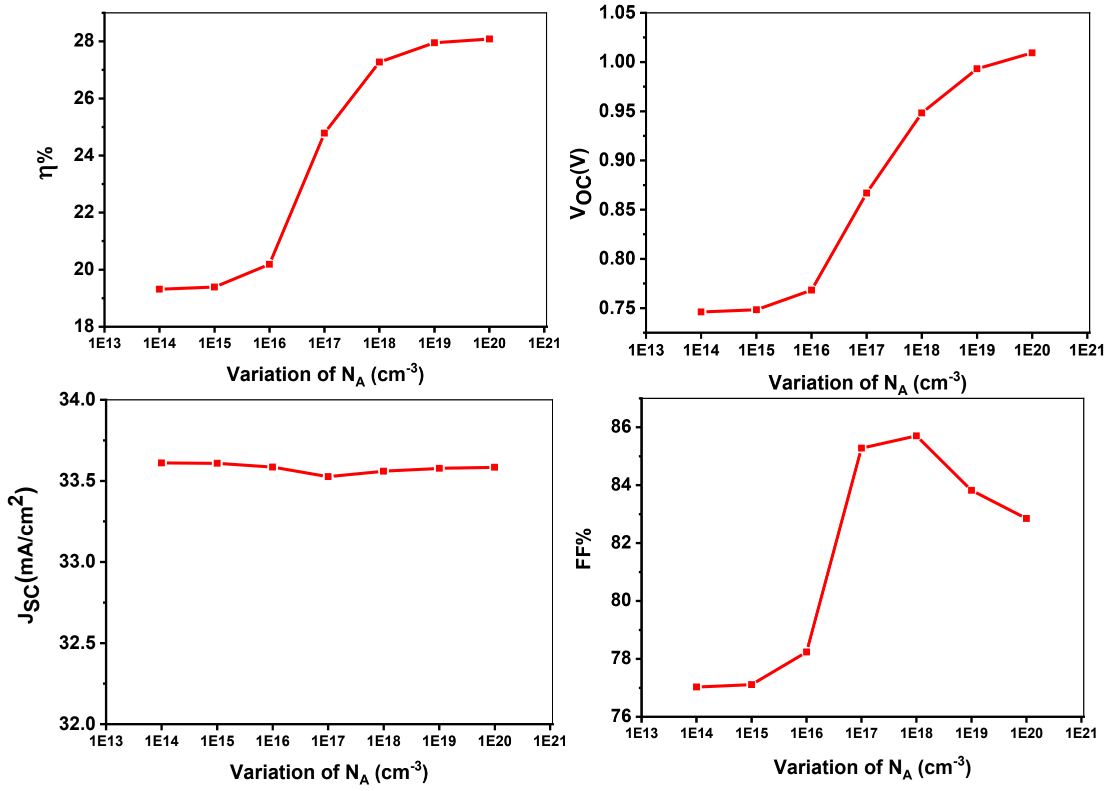

Figure 9: *Variation of efficiency, fill factor, J_{sc}, and V_{oc} with respect to doping density of HTL $MASnI_3$*

3.8 Effect of Doping density N_A of SnS (Absorber material) on Solar cell Parameters

The effect of fixing density (NA) on output electrical characteristics is shown in Figure 10. We found that whereas FF (%), eta (%), and J_{sc} (mA/cm^2) remain almost constant between 1014 and 1020 cm^{-3} and drop after that, V_{oc} (V) marginally increases as doping increases.

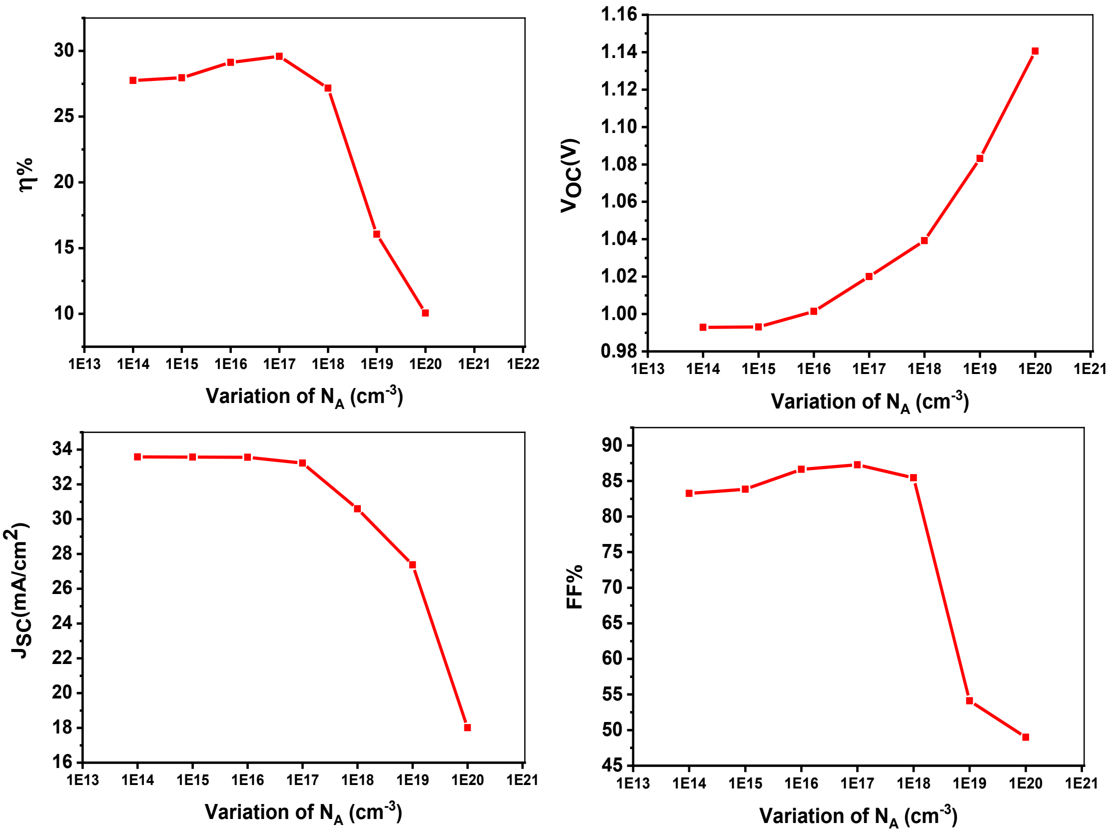

Fig. 10: *Variation of efficiency, fill factor, J_{sc}, and V_{oc} with respect to doping density of SnS (Absorber material).*

3.9 Effect of doping density N_D of ETL (TiO_2) on Solar cell Parameters

The impact of window layer doping (ND) on output electrical characteristics is shown in Figure 11. We found that whereas J_{sc} (mA/cm^2) stays about constant between 1014 and 1020 cm-3 and then starts to decline, FF (%), V_{oc} (V), and conversion efficiency (%) all marginally rise as doping increases. 1018 cm^{-3} is the ideal donor density for ETL.

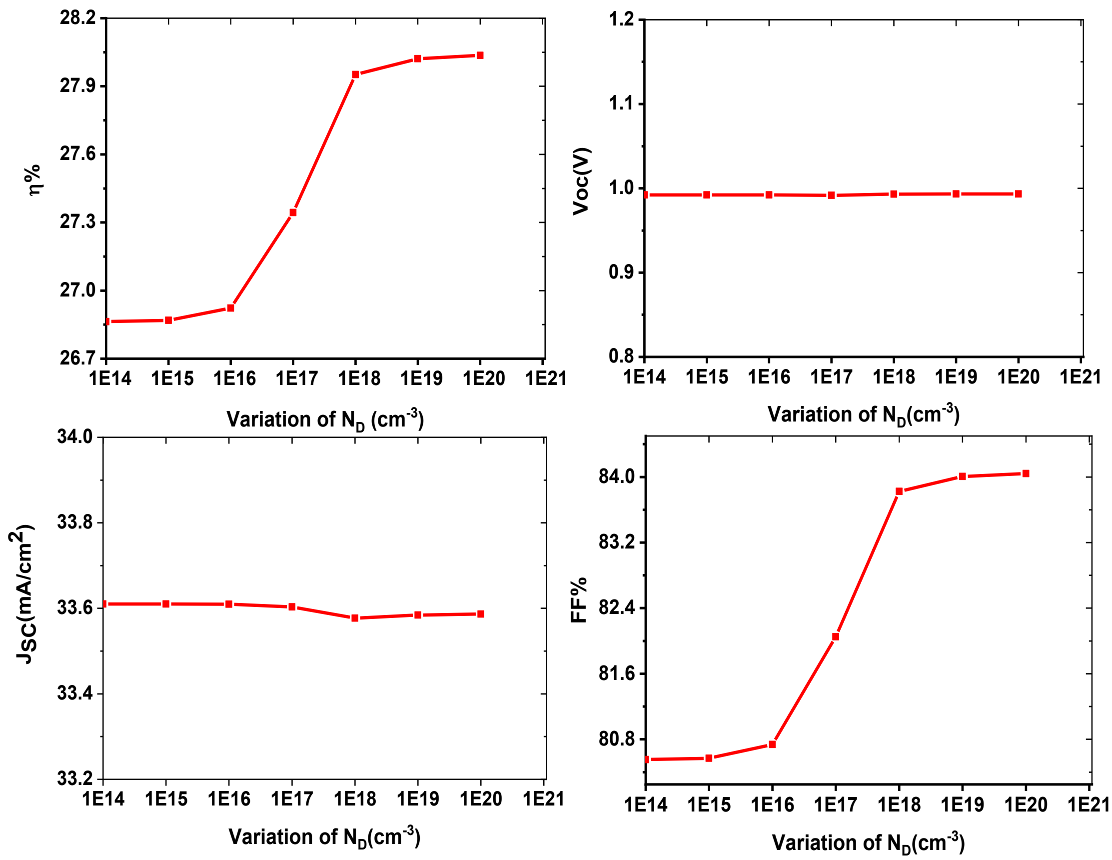

Figure 11: *Variation of efficiency, fill factor, J_{sc}, and V_{oc} with respect to doping density of TiO_2 (ETL)*

4.0 Effect of Temperature (in Kelvin) on Solar Cell Parameters

The output characteristics of the device are significantly influenced by the photovoltaic cell's operating temperature. The operational temperature range for this developed solar cell structure is specified to 275 K to 600 K in this paper. The heterojunction's temperature change is seen in Figure 12. The efficiency falls linearly with rising temperature because the values of V_{oc} and FF decline linearly and J_{sc} increases somewhat. It might be because high temperatures produce enough pairs of electrons and holes to cause charge-carrier recombination, which lowers V_{oc}.

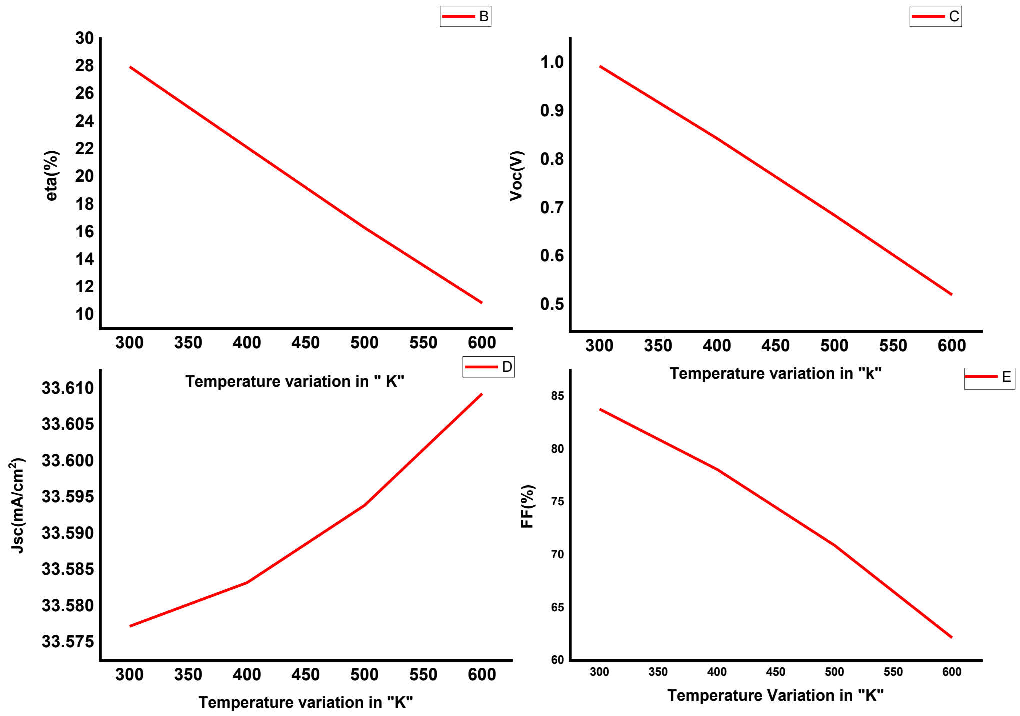

Fig. 12: *Variation of efficiency, fill factor, Jsc, and Voc with respect temperature.*

5. Conclusions

The performance of planar chalcogenide SnS-based perovskite solar cells using TiO_2 as the ETL was summarized in this research, and numerical simulation using the SCAPS program was used to compare the results with other standard ETLs and HTLs. The findings demonstrated that the use of TiO_2 as a substitute ETL has significant potential for PV performance in the FTO/ETL/SnS/$MASnI_3$/Au device design, and that TiO_2 can imitate a PCE of 27.95%. The impact of absorber material thickness was simulated, indicating that using a high absorber layer thickness of 100 nm to 2 µm can yield better results than 100 nm. Moreover, the utilization of Ag, Ni, Mo, and Al as back contacts can facilitate the attainment of a PEC of approximately low. 24.32%, serving as a potential substitute for the costly gold electrode (Au). Our findings will contribute to the optimization of both cost and performance in chalcogenide SnS-based perovskite solar cells. Currently, the research focuses on optimizing the configuration of chalcogenide-based perovskite solar cells through the SCAPS-1D Simulator. This study presents a novel heterojunction SnS-based perovskite structure comprising Au/$MASnI_3$/SnS/TiO_2/FTO, with the optimized thickness values of the various layers of the designed solar cell complete as follows:

Absorber layer SnS = 0.9µm, HTL $MASnI_3$ = 400 nm, and ETL TiO_2 = 20nm.

Furthermore, the optimized values of doping concentrations in different layers are recorded as follows: $MASnI_3$ and SnS acceptor densities are 10^{19} cm^{-3} and 10^{17} cm^{-3}, and the donor density of TiO_2 is 10^{18} cm^{-3}. And the corresponding solar cell performance parameters of the designed solar cell are-V_{oc} (V) = 0.99, J_{sc}(mA/cm^2) = 33.58, FF(%) = 83.82 and η(%) = 27.95.

Conflict of Interest

We certify that there is no variance of importance in the current work.

Acknowledgement

The authors wish to convey their approval to Dr. Marc Burgelman and his team at the University of Gent, within Belgium's Department of Electronics and Information Systems (ELIS), for providing the SCAPS-1D software.

References

1. Crabtree, C. W., & Lewis, N. S. (2005). Basic research needs for solar energy utilization. U.S. Department of Energy, Washington, DC.

2. Crabtree, G. W., & Lewis, N. S. (2007). Solar energy conversion. Physics Today, 60(3), 37–42.

3. Hakes, J. (2000). Long-term world oil supply: A resource base/production path analysis. U.S. Energy Information Administration, Washington, DC.

4. Key, T. (2007). Solar photovoltaics: Expanding electric generation options. Electric Power Research Institute (EPRI), Palo Alto, CA.

5. Wikipedia contributors. (2007). Solar cell efficiency chart. Wikipedia. https://en.wikipedia.org/wiki/Solar_cell

6. Nwofe, P. A., Miles, R. W., & Reddy, K. T. R. (2013). Effects of sulphur and air annealing on the properties of thermally evaporated SnS layers for application in thin-film solar cell devices. Journal of Applied Physics, 113, 011204. https://doi.org/10.1063/1.4791784

7. Ullah, H., & Marí, B. (2014). Numerical analysis of SnS-based polycrystalline solar cells. Superlattices and Microstructures, 72, 148–155. https://doi.org/10.1016/j.spmi.2014.03.042

8. Eperon, G. E., et al. (2014). Perovskite–perovskite tandem photovoltaics. Energy & Environmental Science, 7, 982–988.

9. Yu, Y., Zhao, D., Grice, C. R., Meng, W., Wang, C., Liao, W., Cimaroli, A. J., Zhang, H., Zhu, K., & Yan, Y. (2016). Thermally evaporated methylammonium tin triiodide thin films for lead-free perovskite solar cell fabrication. RSC Advances, 6, 90248–90254. https://doi.org/10.1039/C6RA19476A

10. Fujihara, T., Terakawa, S., Matsushima, T., Qin, C., Yahiro, M., & Adachi, C. (2017). Fabrication of high-coverage $MASnI_3$ perovskite films for stable planar heterojunction solar cells. Journal of Materials Chemistry C, 5, 1121–1127. https://doi.org/10.1039/C6TC05069G

11. Koh, T. M., Krishnamoorthy, T., Yantara, N., Shi, C., Leong, W. L., Boix, P. P., Grimsdale, A. C., Mhaisalkar, S. G., & Mathews, N. (2015). Formamidinium tin-based perovskite with low band gap for photovoltaic applications. Journal of Materials Chemistry A, 3, 14996–15000. https://doi.org/10.1039/C5TA00190K

12. Burgelman, M., Nollet, P., & Degrave, S. (2000). Modelling polycrystalline semiconductor solar cells. Thin Solid Films, 361–362, 527–532. https://doi.org/10.1016/S0040-6090(99)00825-1

13. Verschraegen, J., & Burgelman, M. (2007). Numerical modeling of intraband tunneling for heterojunction solar cells using SCAPS. Thin Solid Films, 515(15), 6276–6279. https://doi.org/10.1016/j.tsf.2006.12.049

14. Degrave, S., Burgelman, M., & Nollet, P. (2003). Modelling of polycrystalline thin-film solar cells: New features in SCAPS version 2.3. Proceedings of the 3rd World Conference on Photovoltaic Energy Conversion, 1, 487–490.

15. Burgelman, M., & Marlein, J. (2008). Analysis of graded band gap solar cells with SCAPS. Proceedings of the 23rd European Photovoltaic Solar Energy Conference, 2151–2155.

16. Michael, P. R., Johnston, D. E., & Moreno, W. (2020). A conversion guide: Solar irradiance and lux illuminance. Journal of Measurements in Engineering, 8(4), 153–166. https://doi.org/10.21595/jme.2020.21667

17. Greulich, J., Höffler, H., Würfel, U., & Rein, S. (2013). Numerical power balance and free energy loss analysis for solar cells including optical, thermodynamic, and electrical aspects. Journal of Applied Physics, 114, 204504. https://doi.org/10.1063/1.4832777.

18. Helander, M. G., Greiner, M. T., Wang, Z. B., Tang, W. M., & Lu, Z. H. (2011). Work function of fluorine-doped tin oxide. Journal of Vacuum Science & Technology A, 29(1). https://doi.org/10.1116/1.3525641

19. Zhou, Y., et al. (2012). A universal method to produce low–work-function electrodes for organic electronics. Science, 336(6079), 327–332. https://doi.org/10.1126/science.1218829.

20. Hwang, J. O., et al. (2012). Work-function-tunable N-doped reduced graphene transparent electrodes for high-performance polymer light-emitting diodes. ACS Nano, 6(1), 159–167. https://doi.org/10.1021/nn203176u.

21. Rahman, S., & Al Ahmed, S. R. (2021). Photovoltaic performance enhancement in CdTe thin-film heterojunction solar cell with Sb_2S_3 as hole transport layer. Solar Energy, 230, 605–617. https://doi.org/10.1016/j.solener.2021.10.036

22. Ahmmed, S., Aktar, A., Hossain, J., & Ismail, A. B. M. (2020). Enhancing the open-circuit voltage of the SnS-based heterojunction solar cell using NiO HTL. Solar Energy, 207, 693–702.

23. Cantas, A., et al. (2018). Importance of CdS buffer layer thickness on Cu_2ZnSnS_4-based solar cell efficiency. Journal of Physics D: Applied Physics, 51(27), 275501. https://doi.org/10.1088/1361-6463/aac8d3

24. Stevanović, V., Hartman, K., Jaramillo, R., Ramanathan, S., Buonassisi, T., & Graf, P. (2014). Variations of ionization potential and electron affinity as a function of surface orientation. Physical Review Applied, 2, 044006.

25. Ahmmed, S., Aktar, A., Hossain, J., & Ismail, A. B. M. (2020). Enhancing the open-circuit voltage of the SnS-based heterojunction solar cell using NiO HTL. Solar Energy, 207, 693–702.

26. Aseena, S., Abraham, N., & Babu, V. S. (2021). Structural and optoelectronic properties of thin-film solar absorber materials. Materials Today: Proceedings. https://doi.org/10.1016/j.matpr.2020.09.077

27. Singh, A. K., Srivastava, S., Mahapatra, A., et al. (2021). Optical and electronic properties of chalcogenide thin films. Optical Materials, 117, 111193. https://doi.org/10.1016/j.optmat.2021.111193

28. Di Mare, S., Menossi, D., Salavei, A., Artegiani, E., Piccinelli, F., Kumar, A., & Romeo, A. (2017). SnS thin-film solar cells: Perspectives and limitations. Coatings, 7(2), 34.

29. Deb, S. K. (2005). Dye-sensitized TiO_2 thin-film solar cell research at the National Renewable Energy Laboratory. Solar Energy Materials & Solar Cells, 88, 1–10. https://doi.org/10.1016/j.solmat.2004.09.007